(NASA-TM-X-3092) AN ASSESSMENT OF AIRFOIL DESIGN BY NUMERICAL OPTIMIZATION (NASA) 33 p HC $3.25 CSCL 01A

N74-28482

Unclas

H1/01 54277

1. Report No.	2. Government Accession No.	3. Recipient's Catalog No.
TM X-3092		

4. Title and Subtitle	5. Report Date
AN ASSESSMENT OF AIRFOIL DESIGN BY NUMERICAL OPTIMIZATION	JULY 1974
	6. Performing Organization Code
7. Author(s)	8. Performing Organization Report No.
Raymond M. Hicks, Earll M. Murman, and Garret N. Vanderplaats	A-5506
	10. Work Unit No.
9. Performing Organization Name and Address	501-06-01
NASA Ames Research Center Moffett Field, Calif. 94035	11. Contract or Grant No.
	13. Type of Report and Period Covered
12. Sponsoring Agency Name and Address	Technical Memorandum
National Aeronautics and Space Administration Washington, D. C. 20546	14. Sponsoring Agency Code

15. Supplementary Notes

16. Abstract

A practical procedure for optimum design of aerodynamic shapes is demonstrated. The proposed procedure uses an optimization program based on the method of feasible directions coupled with an analysis program that uses a relaxation solution of the inviscid, transonic, small-disturbance equations. Results are presented for low-drag, nonlifting transonic airfoils. Extension of the method to lifting airfoils, other speed regimes, and to three dimensions is feasible.

17. Key Words (Suggested by Author(s))	18. Distribution Statement
Optimization Airfoils	Unclassified – Unlimited CAT. 01

19. Security Classif. (of this report)	20. Security Classif. (of this page)	21. No. of Pages	22. Price*
Unclassified	Unclassified	31	$3.25

*For sale by the National Technical Information Service, Springfield, Virginia 22151

NOTATION

c	chord
C_D	section drag coefficient
C_L	section lift coefficient
C_p	pressure coefficient, $\frac{p_1 - p}{q}$
C_p^*	pressure coefficient corresponding to $M_1 = 1$
CT	tolerance for nonlinear constraints
CTL	tolerance for linear constraints
$G(\bar{x})$	constraint function
K	curvature, $\frac{d^2(t/\delta)}{dx^2}\left\{1+\left[\frac{d(t/\delta)}{dx}\right]^2\right\}^{-3/2}$
M	Mach number
M_1	local Mach number
n	degree of polynomial that describes airfoil geometry
$NCON$	number of constraint functions
OBJ	objective function
p	free-stream static pressure
p_1	local static pressure
q	free-stream dynamic pressure
$\bar{s}$	move direction vector
t	thickness
V	area within airfoil contour divided by δ
x	chordwise distance
$\bar{x}$	vector of design variables
y	vertical distance

α scalar move parameter

δ initial airfoil, $\frac{\text{thickness}}{\text{chord}}$

AN ASSESSMENT OF AIRFOIL DESIGN BY NUMERICAL OPTIMIZATION

Raymond M. Hicks, Earll M. Murman, and Garret N. Vanderplaats

Ames Research Center

SUMMARY

A practical procedure for optimum design of aerodynamic shapes is demonstrated. The proposed procedure uses an optimization program based on the method of feasible directions coupled with an analysis program that uses a relaxation solution of the inviscid, transonic, small-disturbance equations. Results are presented for low-drag, nonlifting transonic airfoils. Extension of the method to lifting airfoils, other speed regimes, and to three dimensions is feasible.

INTRODUCTION

At present, there is substantial interest in the design and optimization of airfoil sections for improved aerodynamic characteristics in compressible and incompressible flows. Applications include the development of shock-free sections for maximum supercritical performance, the design of high-lift, low-speed airfoil shapes, and the development of high efficiency aerodynamic bodies.

Many methods have been developed to aid the designer in attaining optimum airfoil sections. Examples include the hodograph method (refs. 1 and 2), an inverse method applied in the physical plane (ref. 3), a combined inverse-direct method (ref. 4), and a numerical optimization method that uses linear theory for supersonic flow and Newtonian theory for hypersonic flow (ref. 5). However, all these methods have limitations. The hodograph procedure is complicated: it requires extensive experience in applied mathematics and theoretical fluid mechanics; it is limited to the development of subcritical or supercritical shock-free, two-dimensional sections; it cannot be readily extended to flows with shocks or three dimensions; and constraints cannot be easily imposed. The inverse method requires *a priori* knowledge of the desirable form of the pressure or velocity distribution and constraints are not readily imposed. The combination inverse-direct method is complicated and requires a designer in the "loop" to monitor and enhance the convergence of the optimization process to a realistic airfoil shape. The numerical optimization method that uses linear or Newtonian theory is not suitable for subsonic- or transonic-flow problems.

This report presents a new application of numerical optimization to the design of airfoil sections. The procedure is not complicated and has none of the above-mentioned limitations. The new procedure uses two existing computer programs – an optimization program based on the method of feasible directions (ref. 6) and an aerodynamic analysis program based on a relaxation solution of the transonic, small-disturbance equations (ref. 7). A brief discussion of both theoretical techniques is given in the appendix. The optimization procedure can be used to design airfoil sections for any speed regime from low speed through supersonic, with realistic constraints. Several examples of the application of this procedure to the design of low-drag, transonic airfoils are presented here. It is feasible to extend the method to other speed regimes and to three-dimensional

design. The results presented here must be considered preliminary and are intended only to illustrate the usefulness and simplicity of the technique.

DESIGN RESULTS AND DISCUSSION

The following numerical optimization problems were considered:

(1) Drag minimization at $M = 0.8$ with geometric and/or flow constraints

(2) Airfoil volume maximization at $M = 0.8$ with drag and geometric constraints

(3) Drag minimization at $M = 0.85$ with geometric constraints

(4) Drag minimization at $M = 1.3$ with geometric constraints

All problems considered are for a nonlifting, symmetric airfoil in inviscid flow. The thickness distributions of the airfoils used are given by either a fourth- or seventh-degree polynomial with a square root leading term (the square root term allows for a blunt leading edge). The coefficients of the polynomials were the design variables perturbed by the optimization program to achieve optimum design. All airfoils are constrained to have no negative thickness.

The first problem considered was to determine whether the optimization procedure could "recognize" a minimum drag contour if a known optimum airfoil were used to start the optimization program. The initial airfoil selected for this problem was a shock-free profile developed by the hodograph method (ref. 1). A least mean-square, seventh-order polynomial was fit to the exact body ordinates. After three perturbations of the geometry, the optimization program returned precisely the same airfoil and pressure distribution as were input (fig. 1).

Case 1: Drag Minimization at $M = 0.8$

An arbitrary airfoil was selected as initial input for this series of optimization problems. The coordinates of the airfoil were given by a seventh-degree polynomial with a square root leading term. The effect of imposing volume constraints ranging from 0 (unconstrained) to 0.7 is shown in figures 2 through 5. For the unconstrained, $V \geq 0.4$ and $V \geq 0.6$ problems (figs. 2–4), the optimization program decreased the volume and thickness of the airfoil until minimum wave drag ($C_D \sim 0$) was achieved. Note that minimum wave drag was attained without eliminating supercritical pressures over the airfoil surface. The volumes of the final airfoils for the constraints $V \geq 0.4$ and $V \geq 0.6$ (figs. 3 and 4) are somewhat larger than that for the unconstrained case (fig. 2), which indicates that the volume constraint had an effect on the final shape even though the final volume was always greater than the constraint value. When the volume constraint was increased to 0.7 (fig. 5), drag was reduced by recontouring the airfoil more, and the final volume was increased over the initial value. For the smaller values of volume constraint, drag was reduced mainly by decreasing the airfoil thickness. The final pressure distribution resulting from a volume constraint of 0.7 exhibits a shock near the 40-percent chord station and therefore a higher drag coefficient than those

cases with smaller volume constraints. Hence, for this class of airfoils, the value of the volume constraint must be considered carefully.

The effect of including a constraint on the local curvature, K, of the airfoil surface along with a volume constraint of 0.7 is shown in figures 6 and 7. Constraining the absolute value of the curvature to less than or equal to 3.5 (fig. 6) appears too restrictive since the drag coefficient of the final airfoil is about 50 percent of the starting value rather than near zero (as shown for the previous cases when only a volume constraint was imposed). When the curvature constraint is increased to 3.9 (fig. 7), the drag is reduced more, but the final value is still greater than that achieved with only a volume constraint. Note that for either value of curvature constraint the shock that occurred at the 40-percent chord station for the volume constraint of 0.7 was eliminated.

Figure 8 shows the addition of a thickness constraint with a slightly "relaxed" curvature constraint and a volume constraint of 0.7. This combination of constraints and starting conditions produced the best result of this study. The final airfoil is practically shock-free, it has essentially zero wave drag, it exhibits an isentropic recompression, and it has greater volume than the initial airfoil. It is not yet possible to specify a combination of constraints that will ensure this type of result for any given starting conditions. However, the method is still very useful since most optimization problems undertaken here resulted in substantial drag reductions and realistic airfoil shapes. The design space appears to be either "flat" or to have local minimums. Therefore, the constraints and starting conditions that produce an absolute minimum or a final airfoil with all the desirable features of the airfoil section shown in figure 8 may be generally difficult to achieve until more is learned about the optimization process. The case shown in figure 9 was included to determine the effect of the curvature constraint on the attainment of the shock-free airfoil in figure 8. (The value of the constraint was increased to 100, which is effectively no constraint on curvature.) Clearly, the curvature constraint in figure 8 was not a predominate factor in the optimization process since the final airfoils of figures 8 and 9 are identical.

When the thickness is constrained at 51 percent of the chord instead of 41 percent, with the same volume and curvature constraints as in the preceding case, the final airfoil is not shock-free (fig. 10). Here, the wave drag coefficient was reduced by a factor of nearly 3 and the volume increased by almost 9 percent. In this case, the final airfoil is not shock-free, but it may be an attractive shape to consider in a design problem because of the increased volume.

The effect of imposing constraints on volume and thickness along with a constraint on pressure coefficient is shown in figure 11. The pressure coefficient was constrained to be less than or equal to 0.2 for chordwise stations that correspond to the subsonic region on the aft portion of the airfoil. (The value of 0.2 was chosen because experimental observation has shown this to be a practical upper limit for the trailing-edge pressure coefficient with attached flow.) In addition, the airfoil was allowed to have a blunt, trailing-edge height greater than or equal to 0.04δ. In this case, the optimization program changed the airfoil geometry in such a way that supercritical pressures over the surface of the airfoil were almost eliminated. Note that the airfoil was modified entirely over the rear 55 percent of the chord whereas, with the shock-free case in figure 8, most of the geometric change occurred over the forward 50 percent of the chord. Again, the drag coefficient was reduced substantially along with an increase in volume. Almost the entire value of C_D shown in the figure results from the slightly blunted trailing edge.

The off-design characteristics of the shock-free airfoil (fig. 8) are shown in figure 12. Note the small drag "creep" beginning at about $M = 0.76$ and the rapid drag rise above $M = 0.8$ (design condition). Because of the rapid rise in drag beginning at the design Mach number, an additional constraint on dC_D/dM was imposed. The drag rise between $M = 0.8$ and 0.81 was required to be less than 15 counts (i.e., $(C_{D_{M=0.81}} - C_{D_{M=0.8}}) < 0.0015$). The resulting improved drag characteristics are shown in figure 13. Figure 14 compares the new airfoil geometry and pressure distribution with the original shock-free section. Note the development of a weak shock near the 50-percent chord station of the new airfoil. Despite the weak shock, the drag coefficient is identical for both airfoils at the design Mach number.

Since the shock-free airfoil in figure 8 was developed by use of small-disturbance theory, it was deemed appropriate to calculate the pressure distribution by full potential theory to evaluate the usefulness of the result. A comparison of the two pressure distributions is shown in figure 15. (A description of the full potential theory used for this calculation can be found in ref. 8.) The agreement between the two theories is good, except the full potential theory indicates the development of a weak shock near the 65-percent chord station.

The effect of mesh refinement for the small-disturbance calculation on the pressure distribution and drag coefficient for the shock-free airfoil is shown in figure 16. The difference in the pressure distributions is small and the drag coefficients are identical.

Different initial airfoil sections were used to start the optimization process for two of the next three cases. The NACA 0012 was used for the two drag minimization results shown in figures 17 and 18. Four design variables were used for these cases because the thickness distribution for the NACA four-digit airfoils is given by a fourth-degree polynomial with a square-root term. The final section in figure 17 exhibits a drag reduction of about 50 percent accompanied by a small increase in volume. Because of the relatively small change in airfoil geometry and pressure distribution realized, a constraint tolerance (see the appendix) used in the optimization program was changed and the solution was recalculated (fig. 18). With the new tolerance, a greater change in the airfoil geometry was achieved, which resulted in a greater drag reduction but without a shock-free shape. Note that the final volume is the same as the constraint value.

Another arbitrary airfoil was used to start the optimization process for the next case (fig. 19). The thickness distribution is given by a fourth-degree polynomial with a square-root term. In this case, the drag was reduced considerably with little loss in volume. The results of the three preceding cases indicate that reducing the number of design variables from seven to four yields less attractive final airfoil sections.

Case 2: Volume Maximization at $M = 0.8$

The problem of maximizing volume subject to constraints on drag and geometry is more difficult for the optimization algorithm for three reasons. First, the drag of the initial airfoil is more than eight times larger than the constraint value (see fig. 20). Second, the drag constraint is a nonlinear function of the design variables (the coefficients of the polynomial used to describe the airfoil geometry). Finally, the constraint on drag coefficient severely restricts the number of acceptable airfoils, which makes a feasible solution more difficult to attain. The result of imposing

constraints on drag coefficient and curvature is shown in figure 20. The initial airfoil is the same as that used in the drag minimization problem. For this problem, the constraint on the drag coefficient was precisely satisfied by reducing the airfoil thickness and volume. This result shows the difficulty in maximizing the volume since, with the same initial airfoil, the drag minimization effort (case 1) resulted in airfoils with more volume and less drag. A thickness constraint at 51 percent of the chord has been added in figure 21. This result is more useful since a reduction in drag coefficient was accompanied by an increase in volume and thickness. Again, a better result is obtained by imposing more constraints. This effect was observed in the development of the shock-free airfoil in figure 8 (i.e., the final airfoil developed without a thickness constraint (fig. 7) was less attractive than the final airfoil developed with a thickness constraint (fig. 8)). However, it is impossible to offer general rules concerning the required magnitude or location of a given constraint since changing the thickness constraint to the 41-percent chord station with all other conditions the same as those in figure 21 resulted in a divergence of the optimization process. This is the only problem to date for which this occurred.

Case 3: Drag Minimization at $M = 0.85$

Drag minimization at $M = 0.85$ was investigated by starting the optimization process with the NACA 0012 airfoil, again defined with four design variables. The effect of imposing a volume constraint only is shown in figure 22. In this case, the drag was reduced substantially by recontouring the airfoil considerably while reducing the thickness and volume. The final pressure distribution indicates the beginning of an isentropic recompression followed by a shock wave near the 75-percent chord station. Because of the reduction in thickness noted, an additional constraint on airfoil thickness was imposed in an effort to reduce the drag without decreasing the thickness. The thickness/chord ratio was constrained to be greater than or equal to 0.125 at the 41-percent chord station with the same volume constraint as for the previous case. Figure 23 shows the result of this calculation. After several iterations, the optimization program showed that (within the stated constraints, starting airfoil and flow conditions) the drag could only increase. The final pressure distribution is nearly identical to the starting distribution except for a slightly stronger shock near the trailing edge of the airfoil (which accounts for the increase in drag).

Since previous experimental work has shown that wave drag can be reduced at low lift by use of a blunt trailing edge, the final airfoil from the preceding case (fig. 23) was modified to permit a 0.0024c open trailing edge; the modified shape was used to start the next optimization problem. The volume and thickness constraints used in the preceding problem were again imposed. The final airfoil and pressure distribution are shown in figure 24. Here the change in both airfoil geometry and pressure distribution is larger than in figure 23 and the drag coefficient is reduced by 47 percent. The drag coefficient shown in figure 24 includes a bluntness drag resulting from the open trailing edge. This result is interesting because it shows that, for small increases in trailing-edge bluntness, the wave drag can be made to decrease more rapidly than the bluntness drag increases if the airfoil is appropriately recontoured. This suggests that an optimum trailing-edge bluntness should be sought to minimize the total drag for a given supercritical flow.

Case 4: Drag Minimization at $M = 1.3$

Drag minimization at low supersonic Mach numbers was the final problem investigated. As with the subsonic phase, it was deemed appropriate to establish whether the optimization program would recognize a known optimum contour when the optimum shape was used as initial input. Linear theory shows that minimum wave drag for a given volume is achieved with a parabolic arc (biconvex) airfoil. Hence this shape was used as the starting airfoil for the first supersonic case (fig. 25). After three perturbations of the geometry, the optimization program returned identically the same shape as the starting airfoil. The wave drag coefficient given by the current theory is 0.0242, which compares favorably with 0.0231 from linear theory. Note, however, that the solution indicates a detached bow shock wave, hence the linear theory solution is not valid at this Mach number and thickness ratio. When the nonlinear terms were suppressed in the calculation, the resulting drag coefficient agreed with the linear theory value to within 1 percent.

The NACA 0006 airfoil and another arbitrary airfoil were selected as initial geometry for the next two supersonic optimization problems (figs. 26 and 27). The geometry of the final airfoils was very different, but the drag coefficients were almost identical and differed little from the value given for the parabolic arc airfoil. This result is interesting in that it shows there may be many different airfoils (with blunt or sharp leading edges) that have wave drag coefficients as low as the biconvex airfoil at low supersonic Mach numbers.

CONCLUDING REMARKS

A procedure for the optimum design of airfoils was demonstrated. A principal attraction of the method is its generality. The results presented here are for nonlifting airfoils at transonic and low supersonic speeds. Extension of the technique to other speed regimes, lifting airfoils, and three-dimensional bodies is straightforward, depending on the availability of suitable aerodynamic programs that describe these flow fields.

The following conclusions are made:

(1) The procedure offers a practical means of airfoil design.

(2) The method is efficient and easy to use. Combining the two computer programs and solving the initial test case required less than 4 man hours.

(3) Significant design improvements may be achieved with only moderate geometric changes.

(4) Consideration of off-design conditions is possible. An optimal airfoil with improved efficiency at an off design condition was obtained with little degradation of performance at the design conditions.

Several areas for further work are identified:

(1) Other representations of the body geometry should be explored, including orthogonal polynomials or other orthogonal sets and, possibly, discrete ordinates with smoothness constraints.

(2) The topology of the design space should be analyzed further to determine wheth the space is flat or composed of many local minimums.

(3) Other optimization algorithms particularly well suited to airfoil design should be developed.

(4) Combined structural-aerodynamic optimization should be explored for synthesizing practical vehicles.

Ames Research Center
National Aeronautics and Space Administration
Moffett Field, Calif., 94035, May 2, 1974

APPENDIX

THEORETICAL CONSIDERATIONS

Aerodynamic Analysis

The aerodynamic analysis program uses a relaxation method to solve the partial differential equation that governs the inviscid, transonic, small-disturbance fluid flow. The problem is solved in the physical plane with appropriate boundary conditions specified for the body and the far field. The governing equations are nonlinear and are of mixed elliptic-hyperbolic type. They admit solutions in which the flow is completely subsonic, completely supersonic, or transonic (mixed subsonic, supersonic). Both shock-free flows and embedded-shock flows are possible. The governing partial differential equation is solved by a fully conservative, mixed-finite-difference, line relaxation algorithm. Complete details of the theory and solution procedure are given in references 7 and 9.[1]

The aerodynamic program was modified to fit the requirements of the optimization program, and the two programs were coupled to produce a single optimum design program The airfoil thickness, t, is described by

$$t = \delta(A\sqrt{x} + a_1 x + a_2 x^2 + \cdots, \; a_n x^n)$$

The square-root term yields a parabolic leading edge and δ is the thickness/chord for the initial airfoil. Values for n of 4 and 7 were used during the study. The coefficients $(A, a_1, \cdots, a_n)$ are the unknown design variables perturbed by the optimization program to determine a solution that minimizes drag without violating any constraints (e.g., airfoil thickness). This particular representation of the airfoil geometry is not unique, and other forms such as Fourier series, piecewise polynomials, or orthogonal polynomials are certainly possible choices. Selecting the above parametric form for the airfoil geometry allows fewer design variables to be used and assures that the airfoil shape will be continuous.

During the optimization process, the aerodynamics of many different airfoils must be calculated. However, each airfoil is a small perturbation on the preceding airfoil and hence the flow characteristics of one airfoil provide a good initial estimate to start the calculation for the next airfoil. This process reduces the number of iterations required for convergence of the relaxation technique used to solve the transonic equation, thereby providing an efficient computational process.

The proposed procedure is not limited to symmetric, nonlifting, two-dimensional airfoils in transonic flow. Lifting airfoils, axisymmetric bodies, or three-dimensional configurations operating in speed regimes other than transonic should be admissible problems to the proposed method if an appropriate aerodynamic program that describes the flow around the bodies is substituted for the present transonic, small-disturbance program.

---

[1] Also in Murman, E. M.: and Cole, J. D.: Inviscid Drag at Transonic Speeds. Paper to be presented at the AIAA 7th Fluid and Plasma Dynamics Conference, Palo Alto, Calif., June 1974.

Optimization Process

Numerous optimization algorithms are available in the literature, each with its own special mathematical characteristics. The basic concept common to each is that a sequence of improving designs is obtained, which leads to a final optimum solution that satisfies all imposed constraints unless such a design does not exist.

Mathematically stated, the optimization problem is of the form:

$$\text{Minimize} \qquad OBJ = F(\bar{x})$$

$$\text{Subject to} \qquad G_j(\bar{x}) \leqslant 0 \ , \quad j = 1, NCON$$

where $\bar{x}$ is a vector containing the design variables – in this case, the coefficients of the airfoil thickness function. When drag is to be minimized, OBJ is the value of the drag coefficient, a highly nonlinear implicit function of the design variables. The term $G_j(\bar{x})$ defines the linear and nonlinear constraints on the design and $NCON$ is the total number of such constraints. For example, if the enclosed volume of the airfoil is required to be greater than or equal to a specified value, V_{min}, the corresponding constraint may be written in normalized form as

$$G(\bar{x}) = 1 - V(\bar{x})/V_{min} \leqslant 0$$

For the polynomial representation used for the airfoil shape, the above constraint is a linear function of the design variables. Other constraints considered include minimum thickness and curvature limits at various chordwise stations on the airfoil, maximum pressure coefficient, and off-design drag rise limits.

The optimization program iteratively updates the design so that at iteration $q, \bar{x}^q = \bar{x}^{q-1} + \alpha \bar{s}^q$ where $\bar{s}$ is a vector direction in the n-dimensional design space and the parameter α defines the distance of movement in the direction $\bar{s}$. At iteration $q, \bar{s}$ is determined so that, for an arbitrarily small α, the objective function is decreased (usable direction) and no constraints are violated (feasible direction). If the initial design is not feasible (if it violates one or more constraints), a direction $\bar{s}$ is found that will overcome this constraint violation with minimal increase in the objective function. At any iteration, if one or more constraints are active or violated, the $\bar{s}$ vector is determined by the method of feasible directions (refs. 10–13). If no constraints are active, either a steepest descent or conjugate direction determined using the Fletcher-Reeves algorithm (refs. 14 and 15), is taken as the move direction. A constraint is defined as active if

$$CT \leqslant G_j(\bar{x}) \leqslant |CT|$$

where CT is a small negative number used to identify near zero values of $G_j(x)$. This is required because precise zero is seldom attainable numerically. A constraint is considered inactive if its value is less than CT and violated if it is greater than $|CT|$; CT is the "constraint tolerance."

The optimization algorithms are described in detail in references 10 through 15 and only a brief geometric interpretation is given here to identify the program requirements.

Consider the two-variable design space shown in figure 28 where an initial unconstrained design is prescribed at point A. At this point, the gradient of the objective function is calculated by a finite-difference computation. The initial direction of movement from this point is the direction of steepest descent, $\bar{s} = -\nabla OBJ$. The parameter α is now determined so that OBJ is minimized or a constraint surface is encountered ($G_j(\bar{x}) = 0$) by moving in this direction. If the objective is nonlinear, subsequent directions are determined by the conjugate direction method (ref. 14) until a constraint surface is encountered (point B, in fig. 28). At B, the gradient of both the objective function and the active constraint(s) is required, again calculated by finite-difference computation. The feasible direction algorithm is used to determine $\bar{s}$. In this case, α is determined so that OBJ is minimized in direction $\bar{s}$, a new constraint is encountered, or a currently active constraint is again encountered. If one or more constraints are violated (point C in fig. 28), as is often true for the initial design, a direction is determined that will point toward the feasible region with minimal increase in OBJ, based on gradients of the objective function and all active and violated constraints.

The optimum design program is segmented into three parts: the main program that initializes all design information; CONMIN, which performs the optimization; and the aerodynamic analysis routines to provide function and constraint evaluations. Figure 29 is a block diagram organization. Optimization usually requires less than 15 design iterations. Gradient calculations using finite difference require n aerodynamic analyses per design iteration (n is the number of design variables). The move (one-dimensional search) in direction $\bar{s}$ requires an average of three analyses. Therefore, the maximum total number of aerodynamic analyses should seldom exceed $15n + 45$. The calculations described under Design Results and Discussion were carried out on a CDC 7600 computer. The majority of the results required from 1 to 3 min of CPU time, which corresponds to 50 to 150 separate transonic flow calculations. Most of the transonic relaxation calculations converged in 10 to 30 iterations.

REFERENCES

1. Bauer, F.; Garabedian, P.; and Korn, D.: A Theory of Supercritical Wing Sections with Computer Programs and Examples. Springer-Verlag, 1972.

2. Nieuwland, G. Y.: Transonic Potential Flow Around Quasi-Elliptical Aerofoil Profiles Obtained From Integral Transform Methods. Tech. Rept. T. 172, National Aerospace Laboratory, 1967.

3. Arlinger, B.: Design of Two Dimensional Airfoil Profile With Prescribed Velocity Distribution Using Conformal Mapping. Saab TN 67, Saab Aircraft Co., Linkoping, Sweden, 1970.

4. Steger, Joseph L.; and Klineberg, John M.: A Finite Difference Method for Transonic Airfoil Design. AIAA J., vol. 11, no. 5, May 1973, pp. 628–635.

5. Hague, D. S.; Rozendaal, H. L.; and Woodward, F. A.: Application of Multivariable Search Techniques to Optimal Aerodynamic Shaping Problems. J. Astronaut. Sci., vol. XV, no. 6, Nov.–Dec. 1968, pp. 283–296.

6. Vanderplaats, Garret N.: CONMIN – A Fortran Program for Constrained Function Minimization. NASA TM X-62,282, 1973.

7. Murman, Earll M.; and Cole, Julian D.: Calculation of Plane Steady Transonic Flows. AIAA J., vol. 9, no. 1, Jan. 1971, pp. 114–121.

8. Jameson, Antony: Transonic Flow Calculations for Airfoils and Bodies of Revolution. Grumman Aerodynamics Rept. 390-71, Dec. 1971.

9. Murman, Earll M.: Uniqueness Requirements for Calculated Jump Conditions Across Embedded Shock Waves Based on Relaxation Methods, Comparing to Time Dependent Finite Difference Calculation. Proceedings of the AIAA Computational Fluid Dynamics Conference, Palm Springs, Calif., July 19–20, 1973.

10. Zoutendijk, K. G., Methods of Feasible Directions; A Study in Linear and Non-Linear Programming. (Thesis) Elsevier Publishing Co., Amsterdam, 1960.

11. Vanderplaats, Garret N.; and Moses, Fred: Structural Optimization by Methods of Feasible Directions, Computers Structures, vol. 3, July 1973, pp. 739–755.

12. Kowalik, J. S.: Feasible Directions Algorithms For Solving General Nonlinear Programming Problems, In Structural Design Applications of Mathematical Programming Techniques, AGARDograph 149, Ch. 7, Feb. 1971.

13. Tocher, J. L.; and Karnes, R. N.: Automated Optimal Weight Fully Stressed Large Scale Structural Design of Aircraft, Using Matrix-Mathematical Programming Technique, AIAA Paper 71-361, April 1971.

14. Fletcher, R.; and Reeves, C. M.: Functional Minimization by Conjugate Gradients, Computer J., vol. 7, no. 2, July 1964, pp. 149–154.

15. Fox, Richard L.: Optimization Methods for Engineering Design, Addison-Wesley, Mass., 1971.

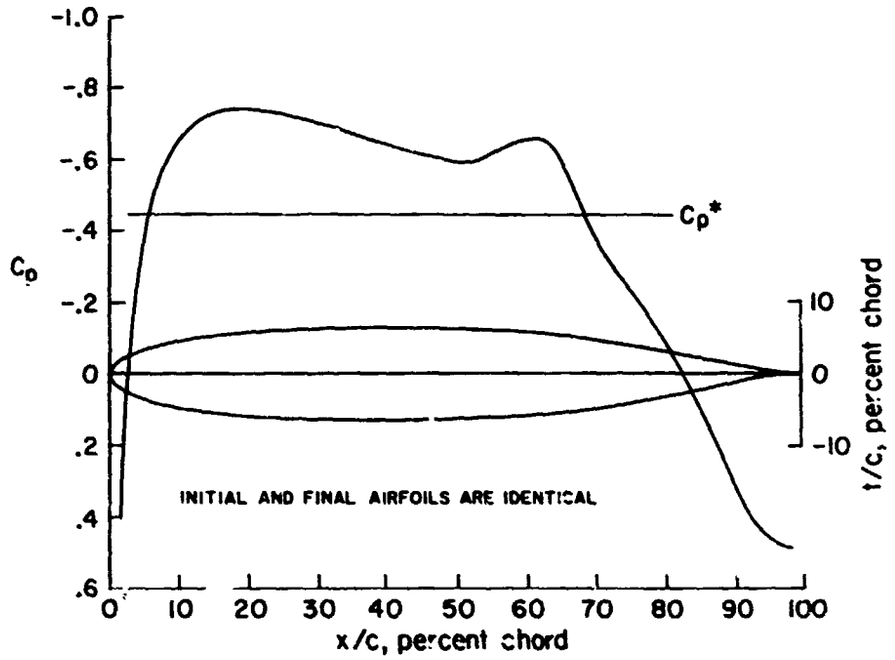

Figure 1.– Drag minimization with known optimum airfoil as initial input. Constraint: $V \geq 0.6$. $n = 7, M = 0.8, C_L = 0, C_D = 0.0007, V = 0.715$.

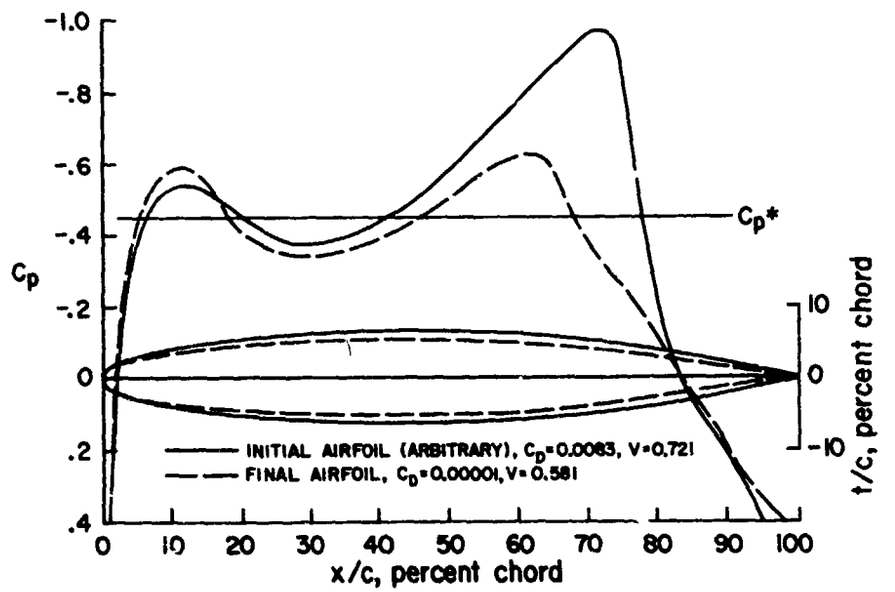

Figure 2.– Drag minimization; unconstrained; $n = 7, M = 0.8, C_L = 0$.

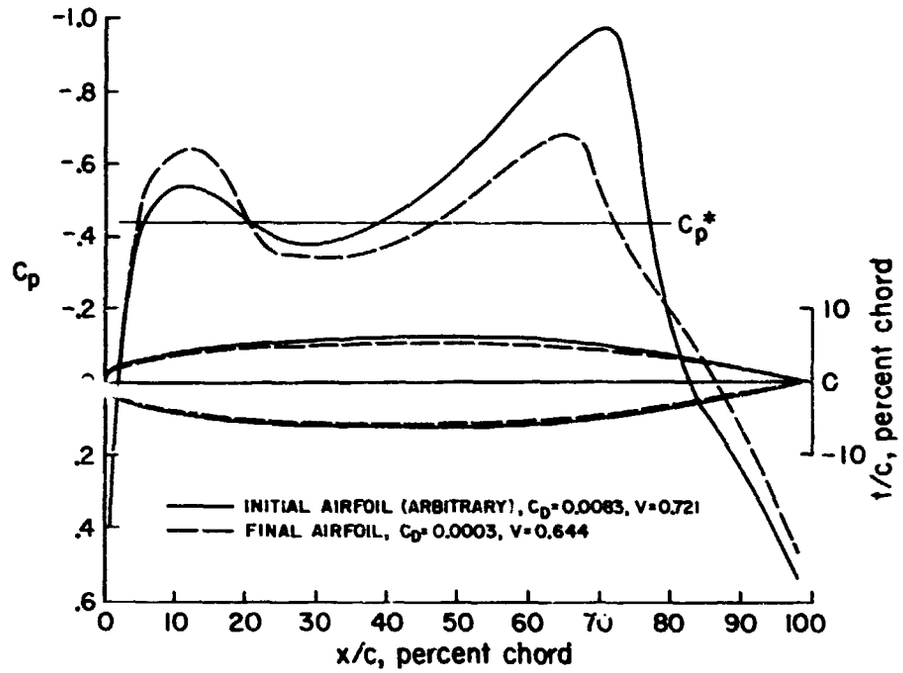

Figure 3.– Drag minimization; constraint: $V \geq 0.4$. $n = 7, M = 0.8, C_L = 0$.

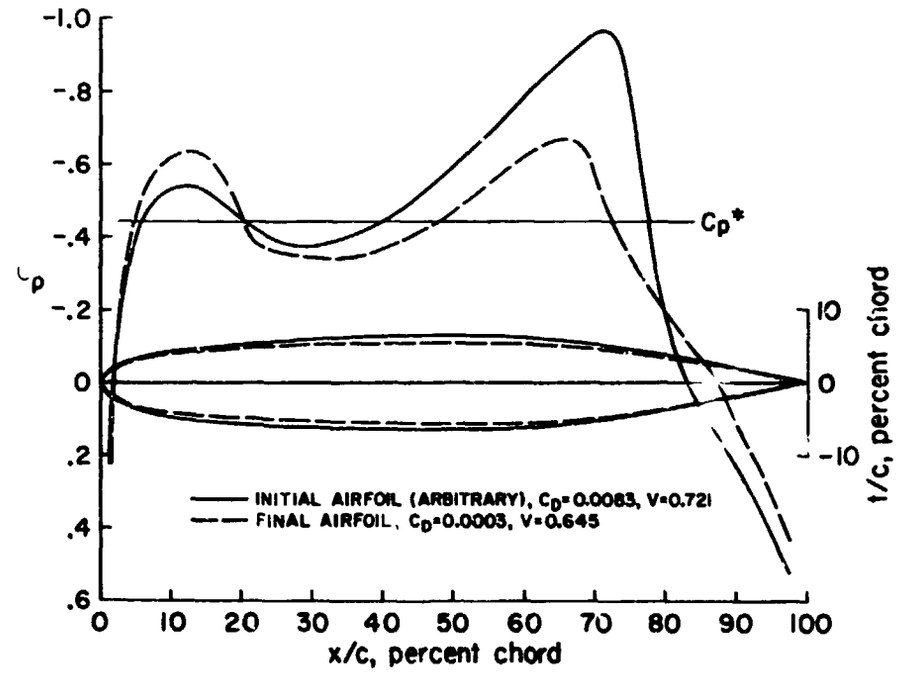

Figure 4.– Drag minimization; constraint: $V \geq 0.6$. $n = 7, M = 0.8, C_L = 0$.

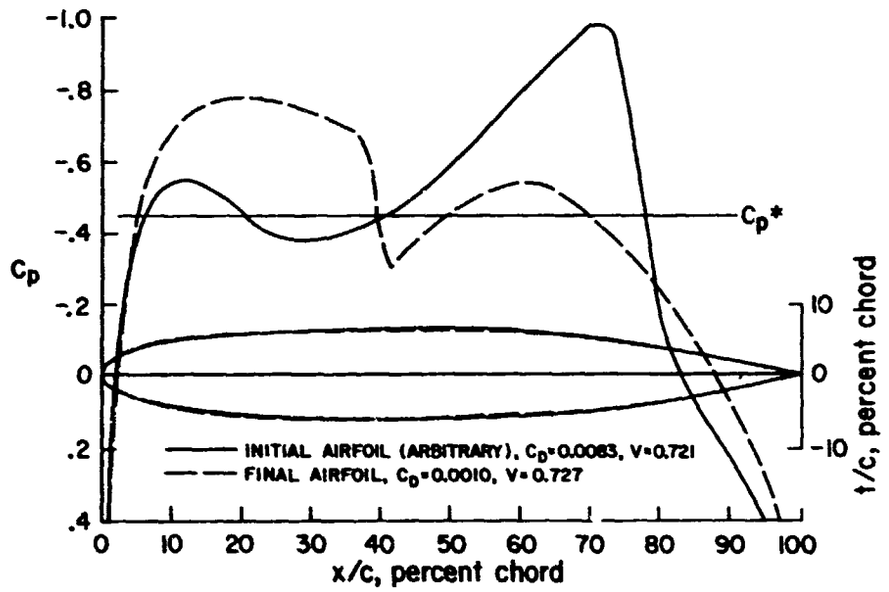

Figure 5.– Drag minimization; constraint: $V \geq 0.7$. $n = 7, M = 0.8, C_L = 0$.

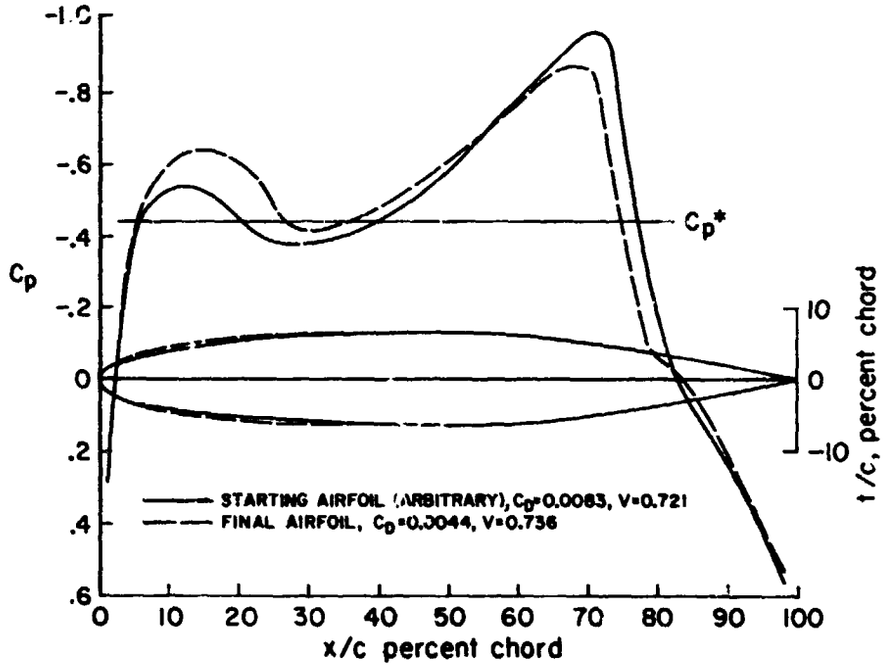

Figure 6.– Drag minimization; constraints. $V \geq 0.7, |K| \leq 3.5$. $n = 7, M = 0.8, C_L = 0$.

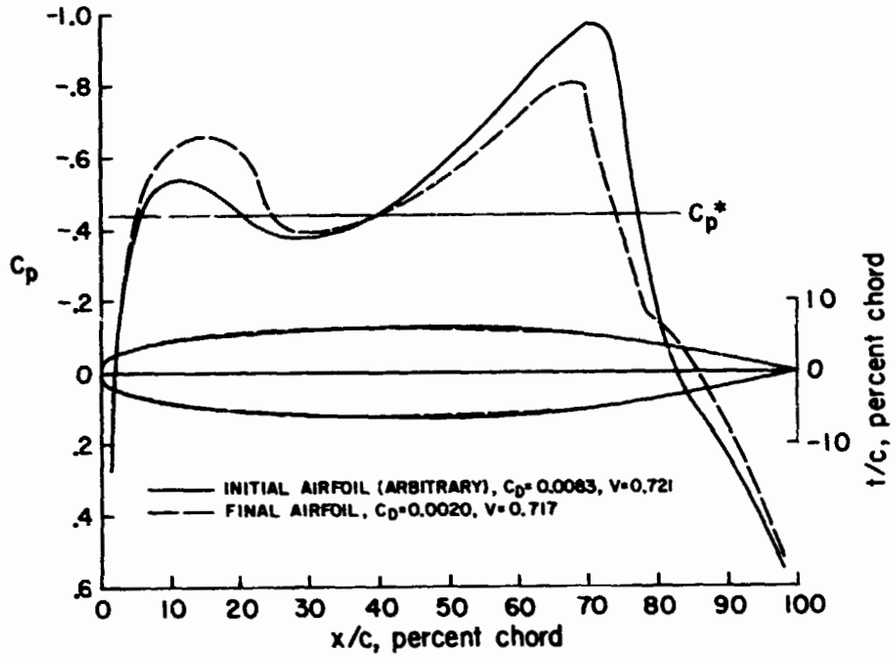

Figure 7.– Drag minimization; constraints: $V \geq 0.7$, $|K| \leq 3.9$. $n = 7, M = 0.8, C_L = 0$.

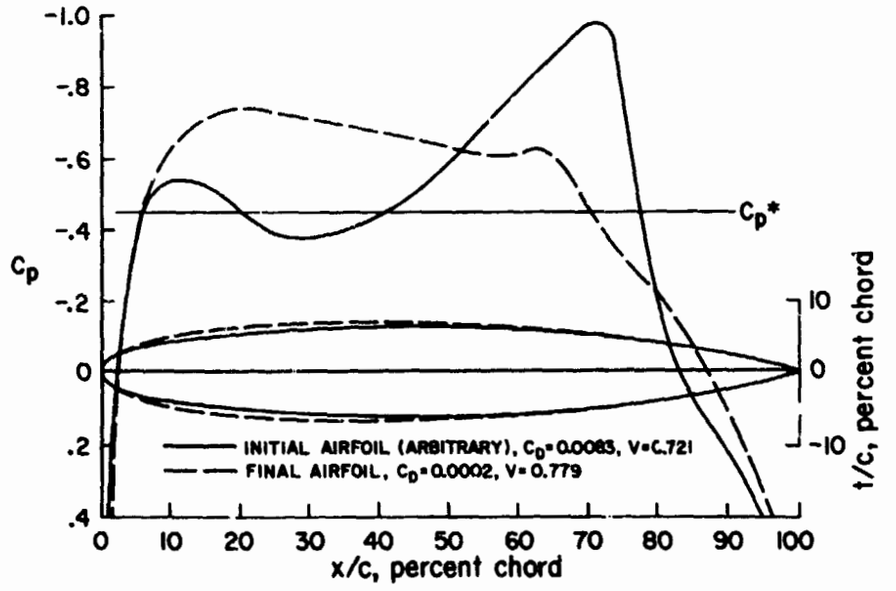

Figure 8.– Drag minimization; constraints: $V \geq 0.7$, $|K| \leq 4.0$, $(t/c) \geq 12.5$ at $(x/c) = 0.41$. $n = 7, M = 0.8, C_L = 0$.

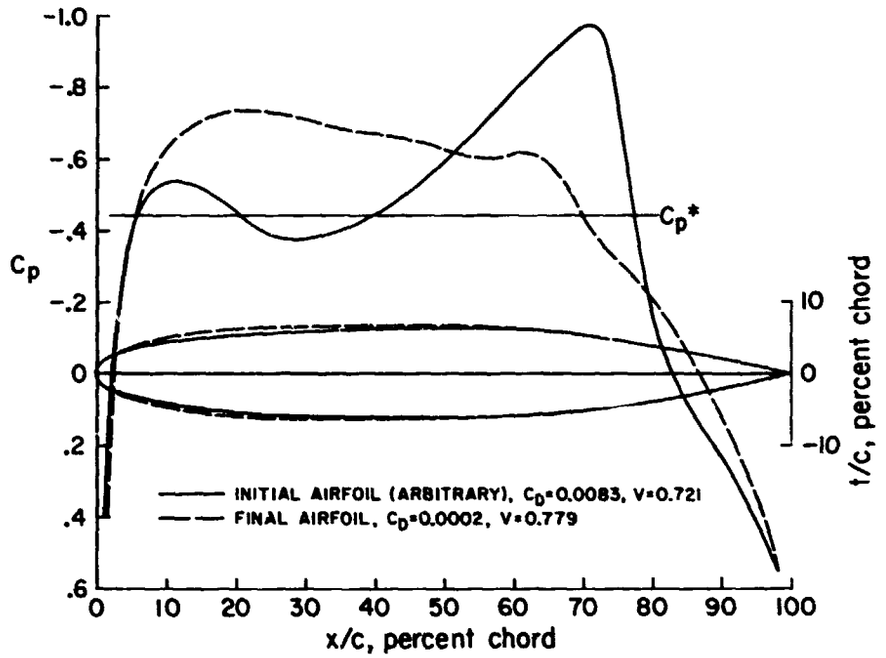

Figure 9.– Drag minimization; constraints: $V \geq 0.7$, $|K| \leq 100$, $(t/c) \geq 12.5$ at $(x/c) = 0.41$. $n = 7, M = 0.8, C_L = 0$.

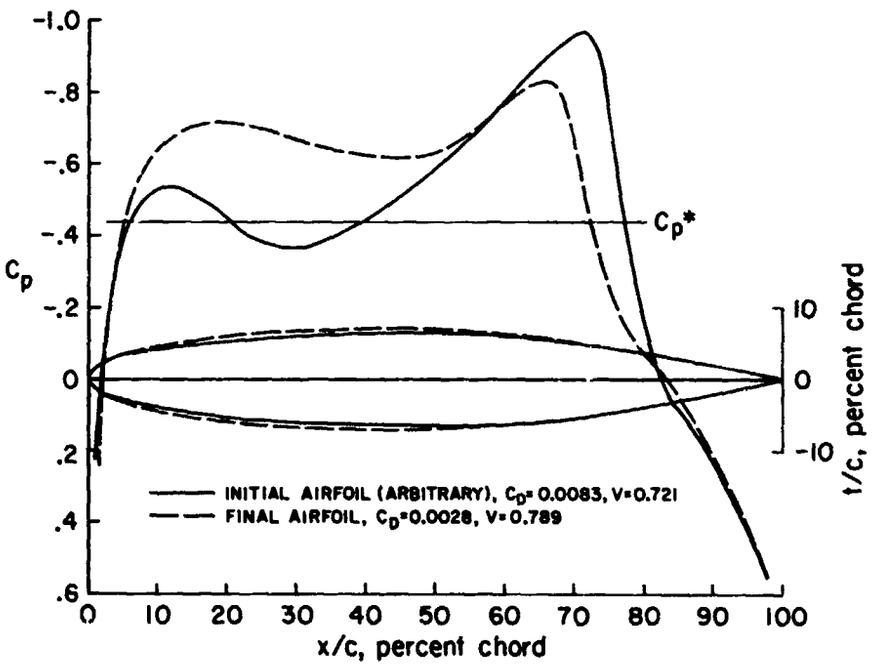

Figure 10.– Drag minimization; constraints: $V \geq 0.7$, $|K| \leq 100$, $(t/c) \geq 12.5$ at $(x/c) = 0.51$. $n = 7, M = 0.8, C_L = 0$.

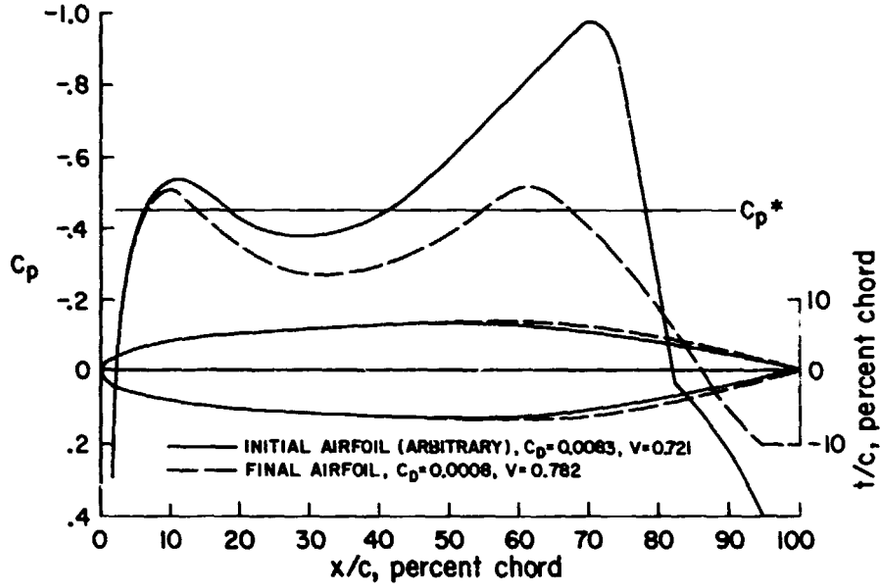

Figure 11.– Drag minimization; constraints: $V \geqslant 0.65$, $(t/c) \geqslant 12.5$ at $(x/c) = 0.41$, $C_p \leqslant 0.2$ for $(x/c) > (x/c)_{C_p^*}$. $n = 7, M = 0.8, C_L = 0$.

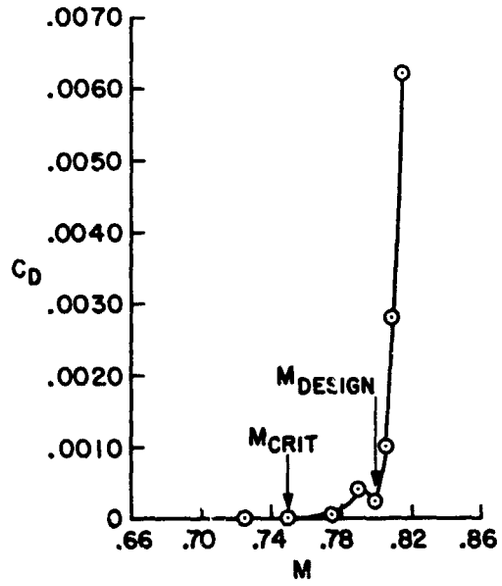

Figure 12.– Drag rise characteristics at shock-free airfoil.

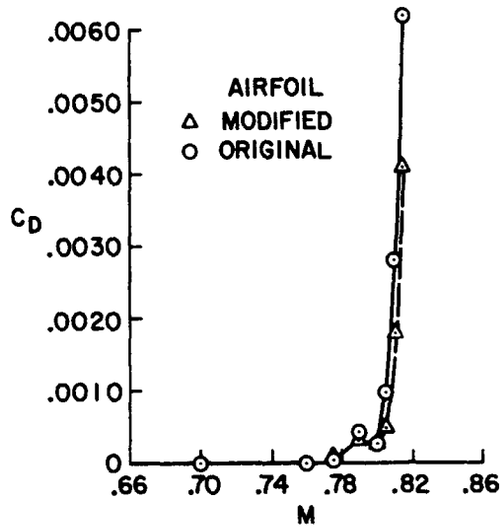

Figure 13.– Drag rise characteristics of shock-free airfoil modified to reduce drag rise.

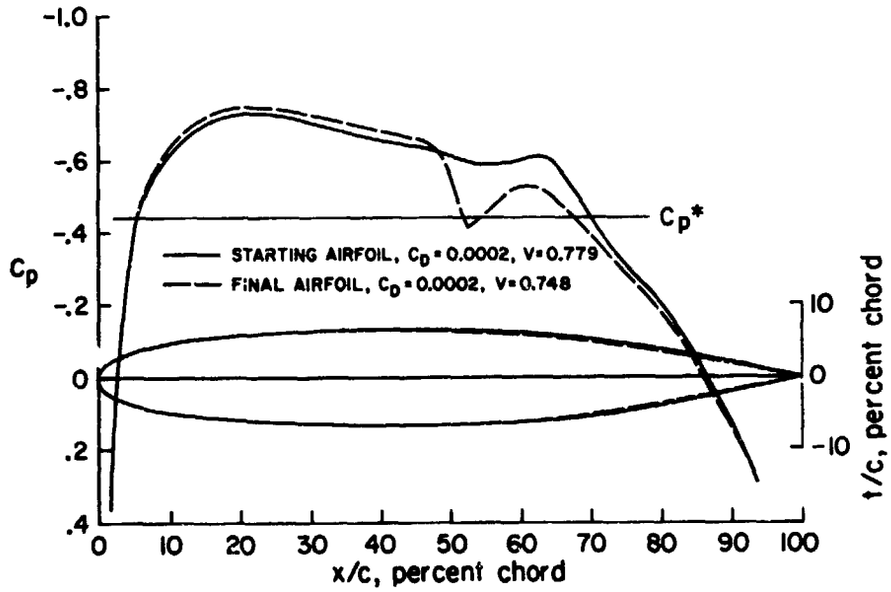

Figure 14.– Drag rise reduction; constraints: $V \geq 0.7$, $|K| \leq 100$, $(t/c) \geq 12.5$ at $(x/c) = 0.41$. $(C_{D_{M=0.81}} - C_{D_{M=0.8}}) \leq 0.0015$. $n = 7$, $C_L = 0$.

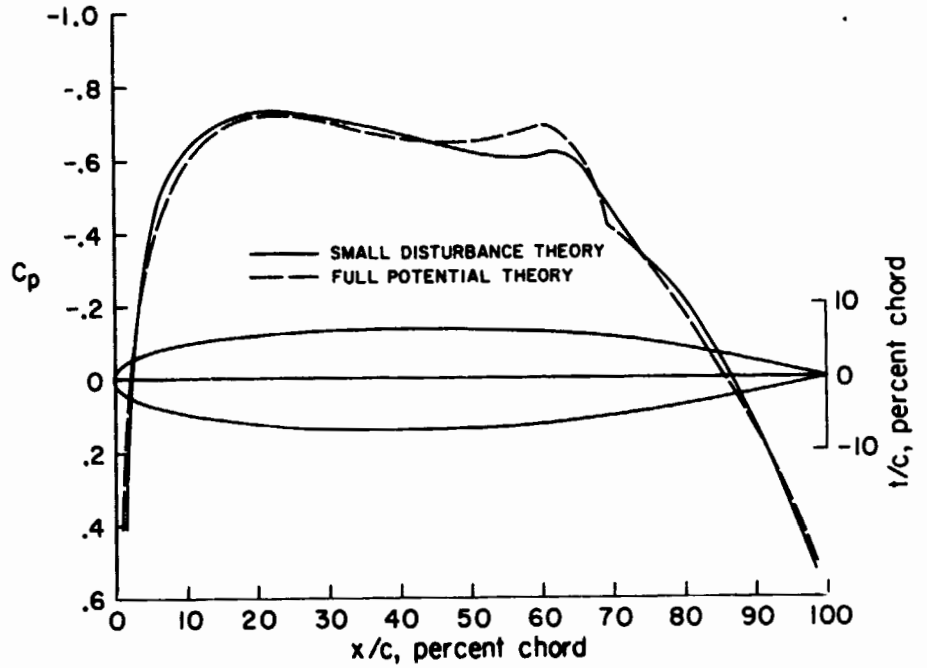

Figure 15.– Comparison of small-disturbance theory with full potential theory for shock-free airfoil, $M = 0.8, C_L = 0$.

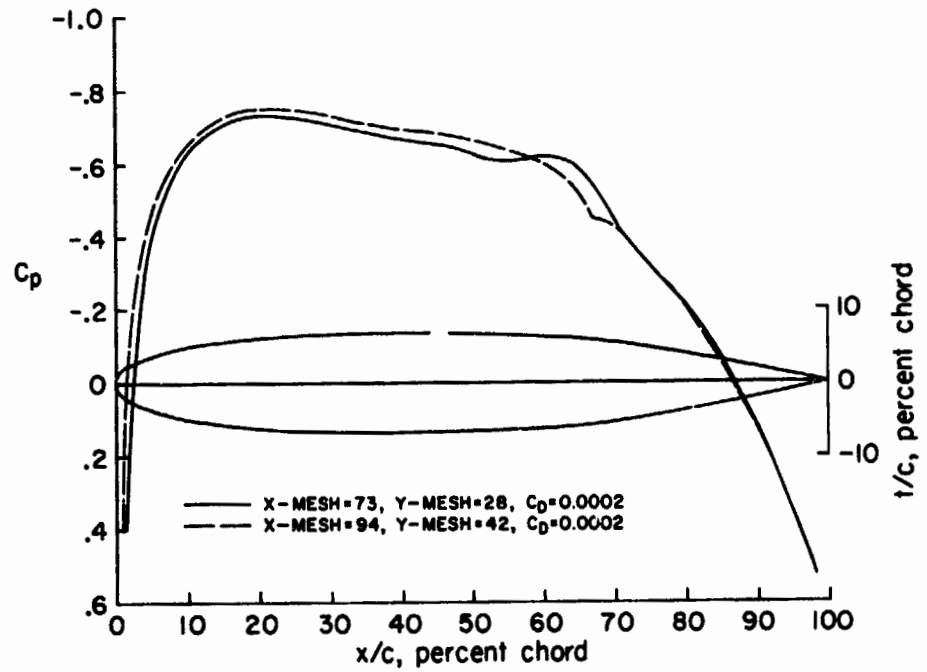

Figure 16.– Effect of mesh spacing on pressure distribution and drag for shock-free airfoil, small-disturbance theory; $M = 0.8$.

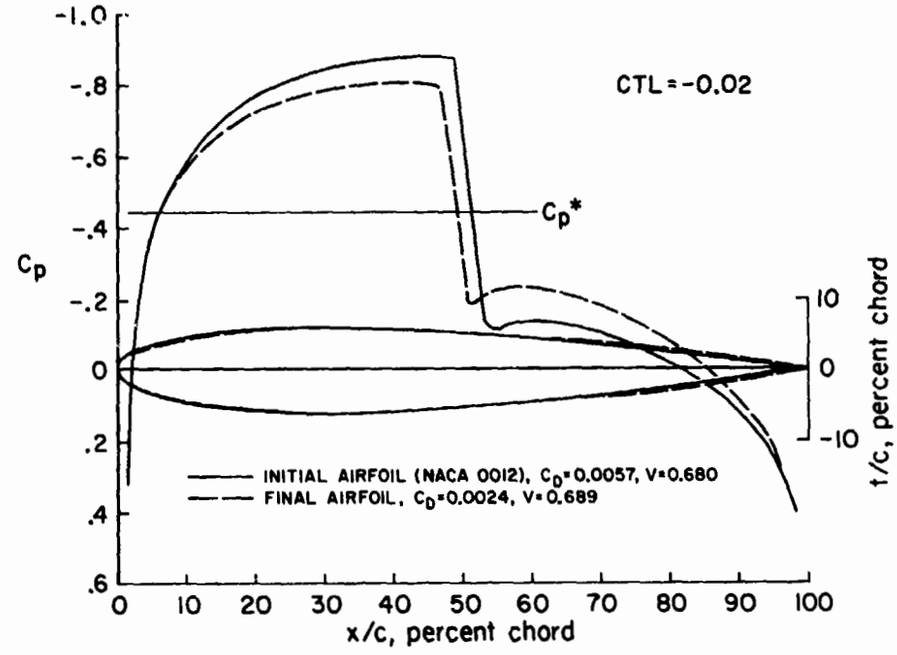

Figure 17.– Drag minimization; constraint: $V \geq 0.65$. $n = 4, M = 0.8, C_L = 0$.

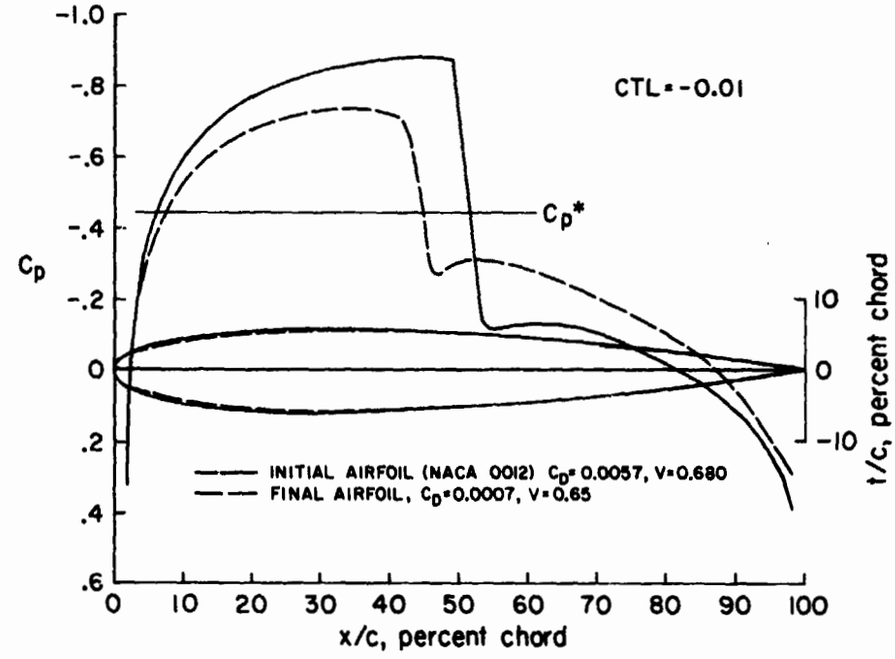

Figure 18.– Drag minimization; constraint: $V \geq 0.65$. $n = 4, M = 0.8, C_L = 0$.

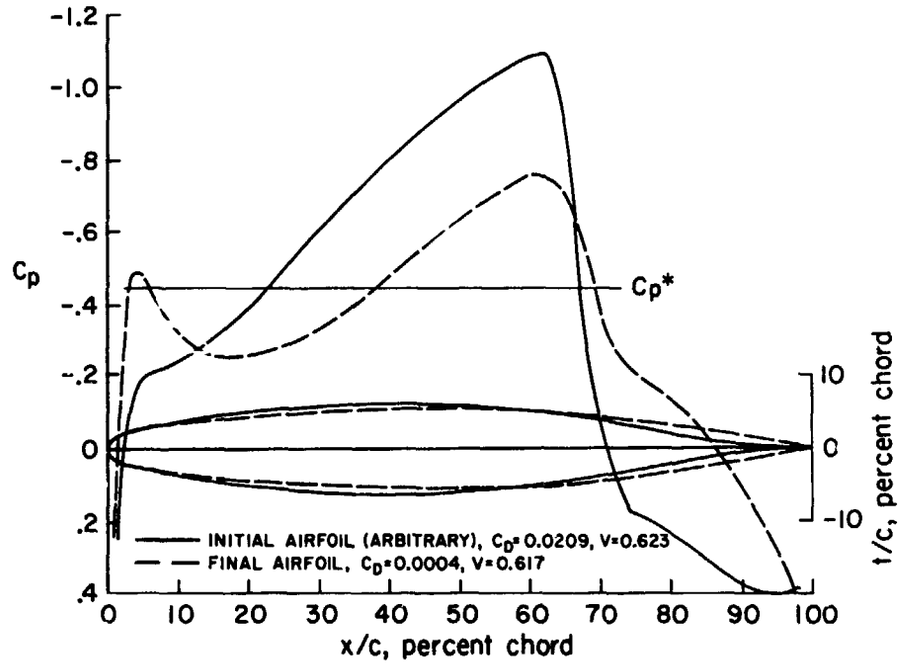

Figure 19.– Drag minimization; constraint: $V \geqslant 0.6$. $n = 4, M = 0.8, C_L = 0$.

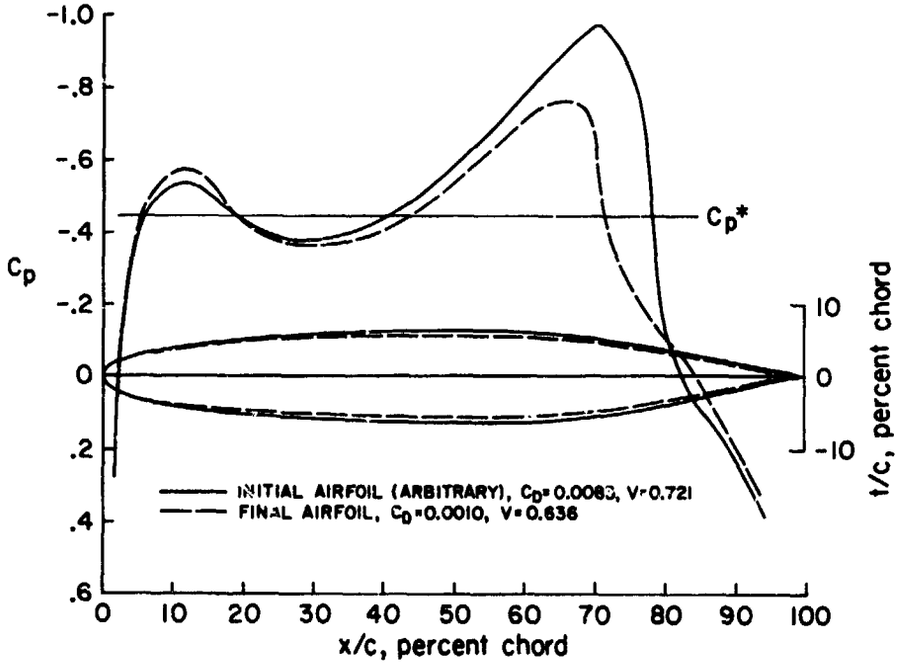

Figure 20.– Volume maximization; constraints: $C_D \leqslant 0.001, |K| \leqslant 100$. $n = 7, M = 0.8, C_L = 0$.

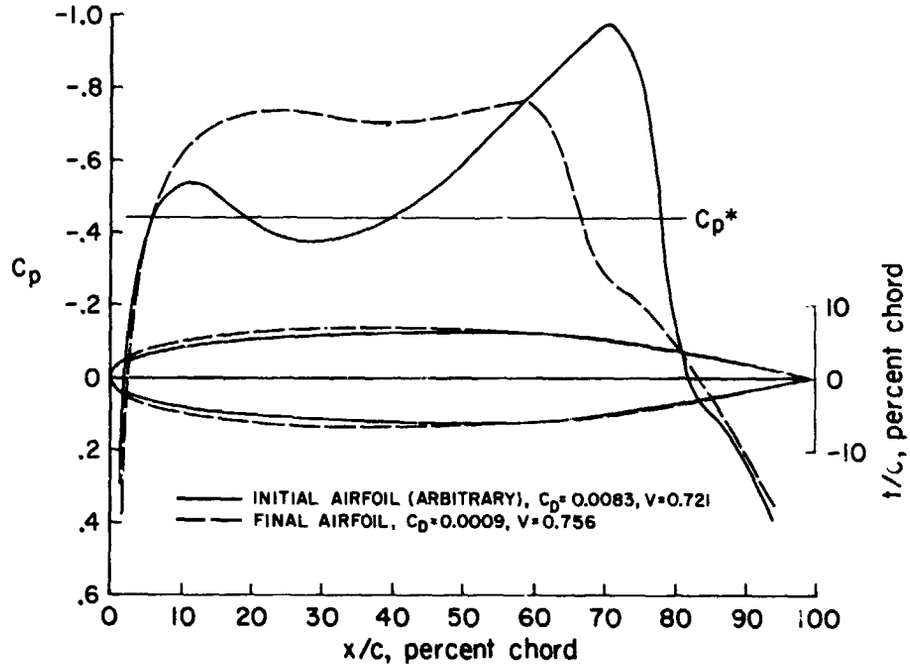

Figure 21.– Volume maximization; constraints: $C_D \leqslant 0.001$, $|K| \leqslant 100$, $(t/c) \geqslant 12.5$ at $(x/c) = 0.51$. $n = 7, M = 0.8, C_L = 0$.

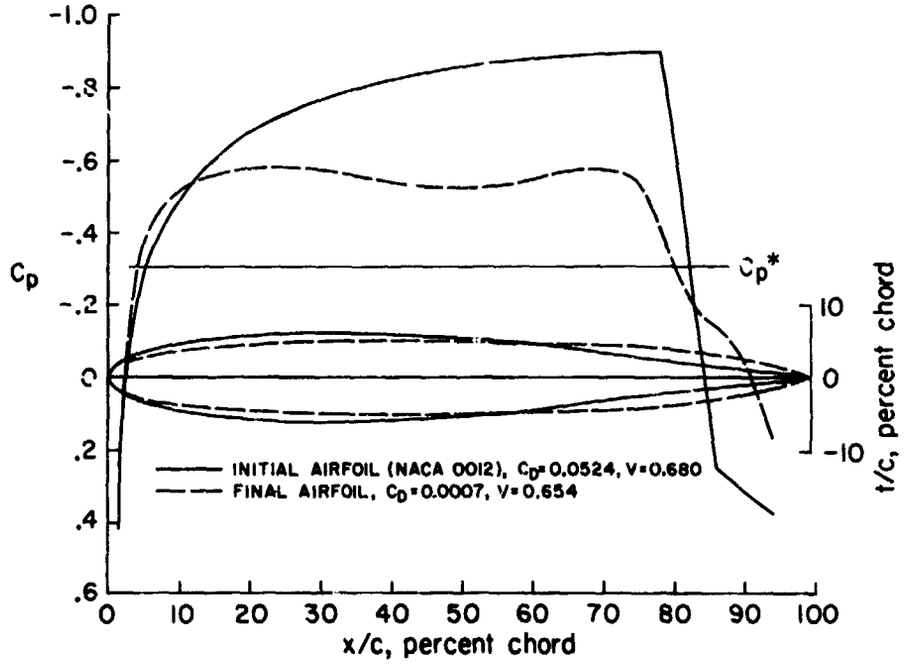

Figure 22.– Drag minimization; constraint: $V \geqslant 0.65$. $n = 4, M = 0.85, C_L = 0$.

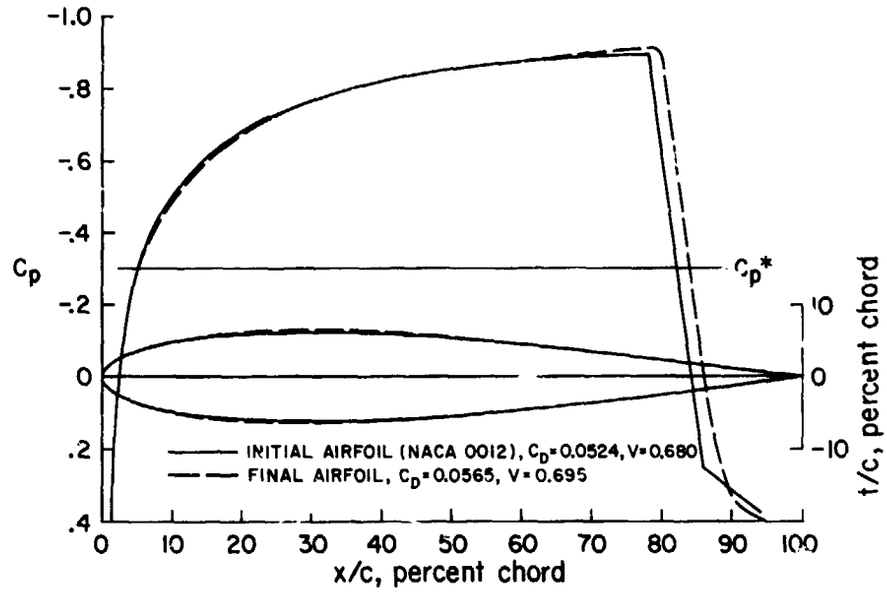

Figure 23.– Drag minimization; constraints: $V \geq 0.65$, $(t/c) \geq 12.5$ at $(x/c) = 0.41$. $n = 4, M = 0.85, C_L = 0$.

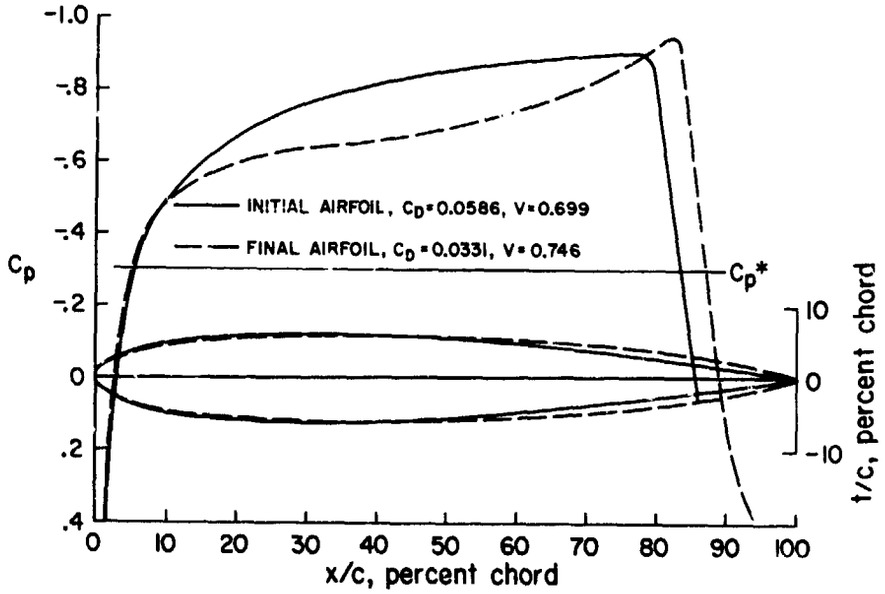

Figure 24.– Drag minimization; constraints: $V \geq 0.65$, $(t/c) \geq 12.5$ at $(x/c) = 0.41$. $n = 4, M = 0.85, C_L = 0$.

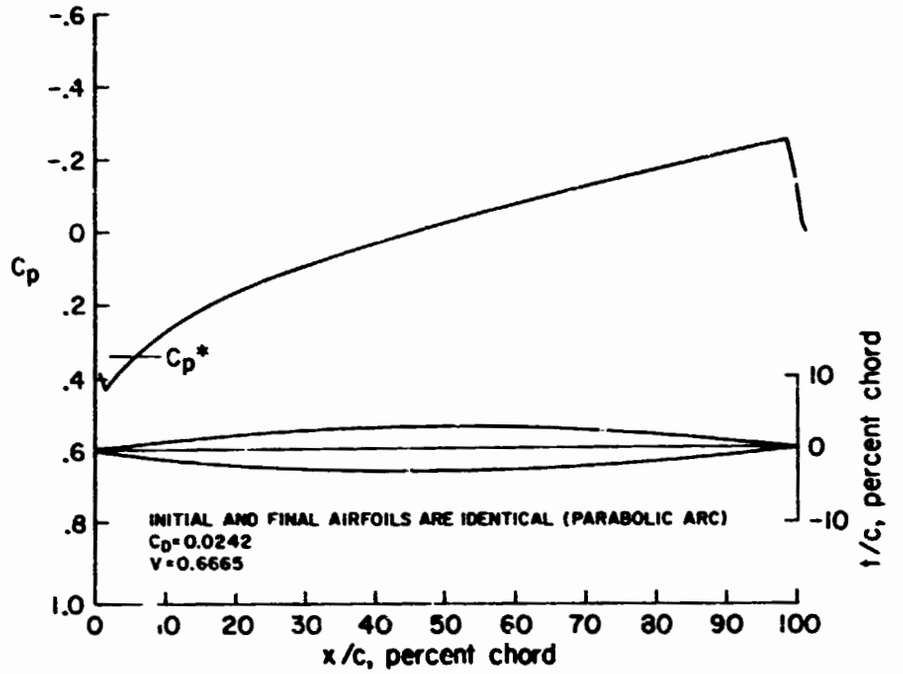

Figure 25.– Drag minimization with known optimum airfoil as initial input. Constraint: $V \geq 0.665$. $n = 4, M = 1.3, C_L = 0$.

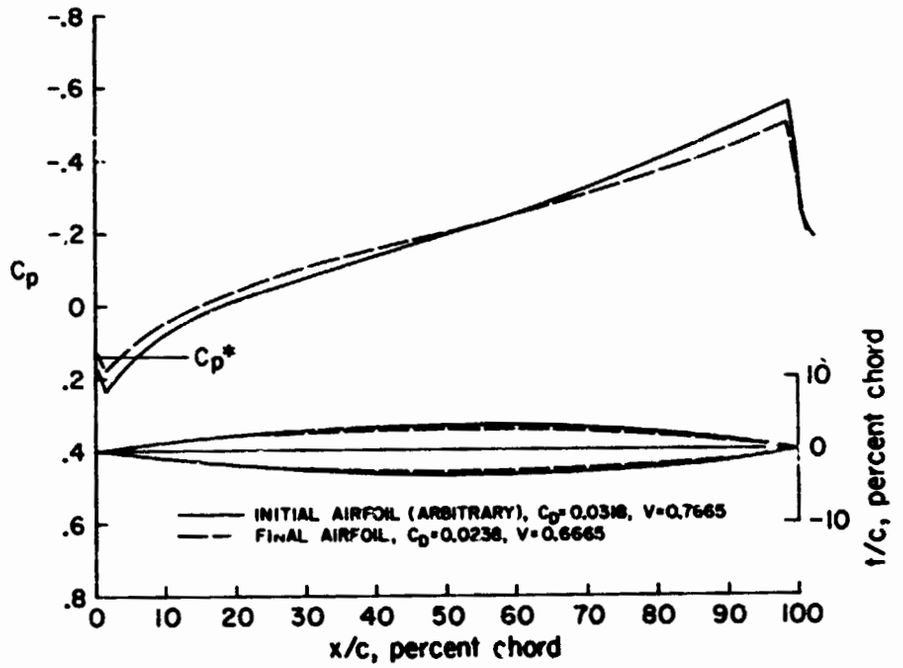

Figure 26.– Drag minimization with detached shock. Constraint: $V \geq 0.6665$. $n = 4, M = 1.3, C_L = 0$.

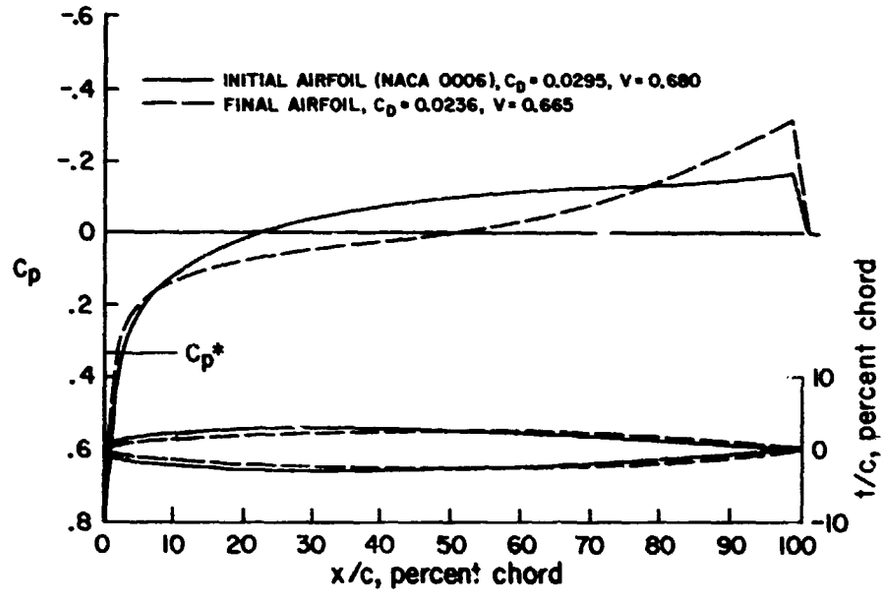

Figure 27.– Drag minimization with detached shock. Constraint: $V \geq 0.665$. $n = 4, M = 1.3, C_L = 0$.

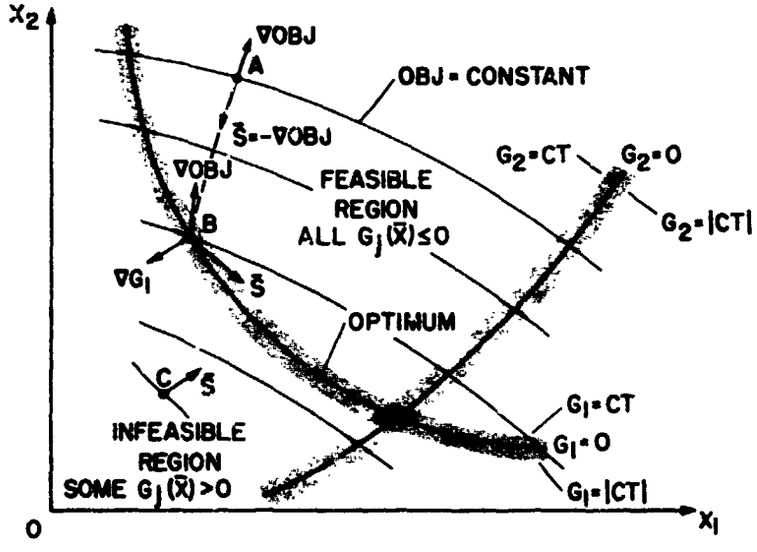

Figure 28.– Two variable design space.